Supplementary Information

3.88 Å structure of cytoplasmic polyhedrosis virus by cryo-electron microscopy

Xuekui Yu[1], Lei Jin[1], Z. Hong Zhou[1,2,*]

[1]Department of Pathology and Laboratory Medicine,
The University of Texas Medical School at Houston,
Houston, Texas 77030, USA; [2]Department of Microbiology, Immunology & Molecular Genetics and The California NanoSystems Institute, University of California at Los Angeles, Los Angeles, CA 90095-1594, USA

***Corresponding author: Hong.Zhou@UCLA.edu** Phone: **310-206-0033;** Fax: **310-206-5365**

Functional implications of the conformational change between CSP-A and CSP-B

The genomic dsRNA is coiled and tightly packed within the capsid with a multilayer arrangement. The outmost RNA layer interacts with the inner side of the capsid shell (Fig. 2d). We identified three shallow grooves in the inner sides of both the CSP-A and CSP-B that are ~27 Å apart. All three grooves are well aligned between CSP-A and CSP-B (Supplementary Fig. 7 and Supplementary Movie 5), which may function as tracks for RNA packing, similar to the proposed model described in BTV-based crystallographic investigations[1]. The current belief is that single-stranded mRNAs (ssRNA) are encapsulated within the nascent core[2]. It is possible that the conformational change occurs at the genome replication stage during capsid assembly, when mRNAs are used as templates for minus-strand synthesis to produce dsRNA segments. During this stage of RNA replication, RNA template sliding and the increased electrostatic repulsion may trigger the conformational change. In CSP-A, the α-helix (residues 1014-1024, green in Supplementary Fig. 7) is located between the two upper grooves and might function as a spacer for adjacent RNA duplexes. In CSP-B, this α-helix would sit on the track of the middle groove, affecting RNA packing and blocking its sliding, were it not restructured (Supplementary Fig. 7). Thus, the helix-to-β-hairpin conformational change we observed provides a direct piece of structural evidence associated with RNA packing and sliding. If this is indeed the case, then the path of changing (indicated by the empty arrow in Fig. 2c) may provide a hint about the sliding direction of the RNA template, which is clockwise when viewed from inside the capsid along the five-fold axis (Supplementary Fig. 7).

Supplementary Table 1 Data Acquisition and Processing Statistics

	Far-from-focus	*Close-to-focus*
CCD frames used	1,615	1,304
Particles included	17,125	12,814
Defocus range (μm)	1.63-2.78	0.15-1.3
B-factor (Å^2)	Not measured	35
Resolution (Å)	Not measured	3.88

Legends for Movies:

Supplementary Movie 1 Overall structure of the CPV capsid at 3.88-Å resolution.

Supplementary Movie 2 An extracted helical density from CSP-B superimposed with the Cα trace of a standard α-helix, showing the clear turns, the deep grooves and the densities for side-chains revealed by the cryoEM map.

Supplementary Movie 3 An extracted density superimposed with the Cα traces of CSP-A, showing the separation of the two β strands.

Supplementary Movie 4 An extracted asymmetric unit from the 3.88-Å resolution density map.

Supplementary Movie 5 Density map of CSP-A (blue) and CSP-B (purple) with dsRNA models (red), showing three shallow grooves in the inner sides of both CSP-A and CSP-B. All three grooves are well aligned between CSP-A and CSP-B, forming sliding tracks for RNA.

Supplementary Movie 6 One TP pentamer (gray), showing that the central chamber of the turret is plugged in by the hemagglutinin-like "A spike" (yellow density).

Supplementary Movie 7 Cα models of one CSP-B (cyan), two CSP-As (red and orange), and two GTase domains (blue and light blue), showing the mRNA releasing and capping pathway.

Supplementary Movie 8 Shaded surface representation of TP, showing the two methylase domains (purple), GTase domain (blue), and CPV's unique polyhedrin-binding domain (orange).

Supplementary Movie 9 View of one entire turret, showing the orientation and position of one TP in the turret.

References:

1. Gouet, P. et al. The highly ordered double-stranded RNA genome of bluetongue virus revealed by crystallography. Cell 97, 481-490 (1999).
2. Grimes, J. M. et al. The atomic structure of the bluetongue virus core. Nature 395, 470-478 (1998).
3. Kraulis, P. J. MOLSCRIPT: a program to produce both detailed and schematic plots of protein structures. J. Appl. Crystallogr. 24, 946-950 (1991).
4. Reinisch, K. M., Nibert, M. L. & Harrison, S. C. Structure of the reovirus core at 3.6 Å resolution. Nature 404, 960-967 (2000).

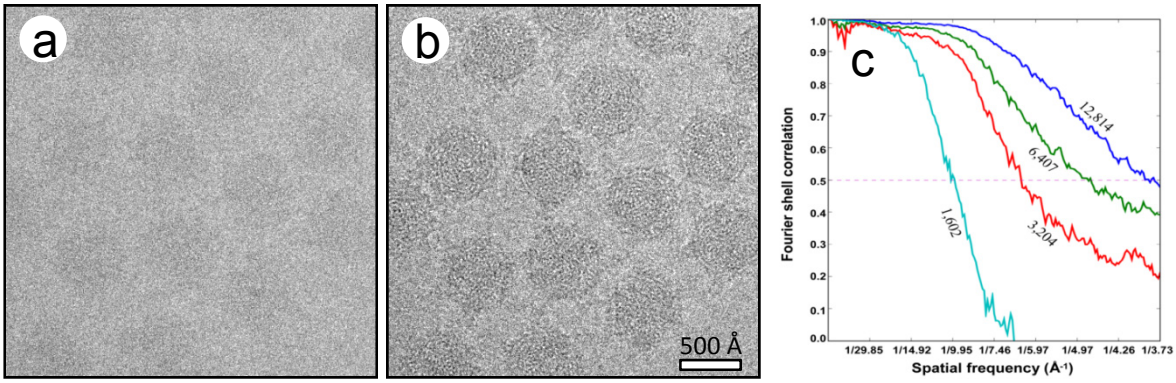

Supplementary Figure 1 **Cryo-electron microscopy and resolution assessment. a**, **b**, A representative area of the first, close-to-focus CCD micrograph (**a**) and the second, far-from-focus CCD micrograph (**b**) of a focal pair of ice-embedded CPV capsids recorded on a 16 megapixel TVPIS CCD in a FEI Polara 300kV instrument with a FEG at liquid nitrogen temperature. The defocus values were determined to be 0.35 µm and 1.83 µm underfocus for **a** and **b**, respectively. **c**, Fourier shell correlation plot, showing the effective resolution of our 3D reconstruction improved as the number of particles included increased, reaching 3.88 Å for the final data set of 12,814 particles using the criterion of 0.5 Fourier shell correlation coefficient.

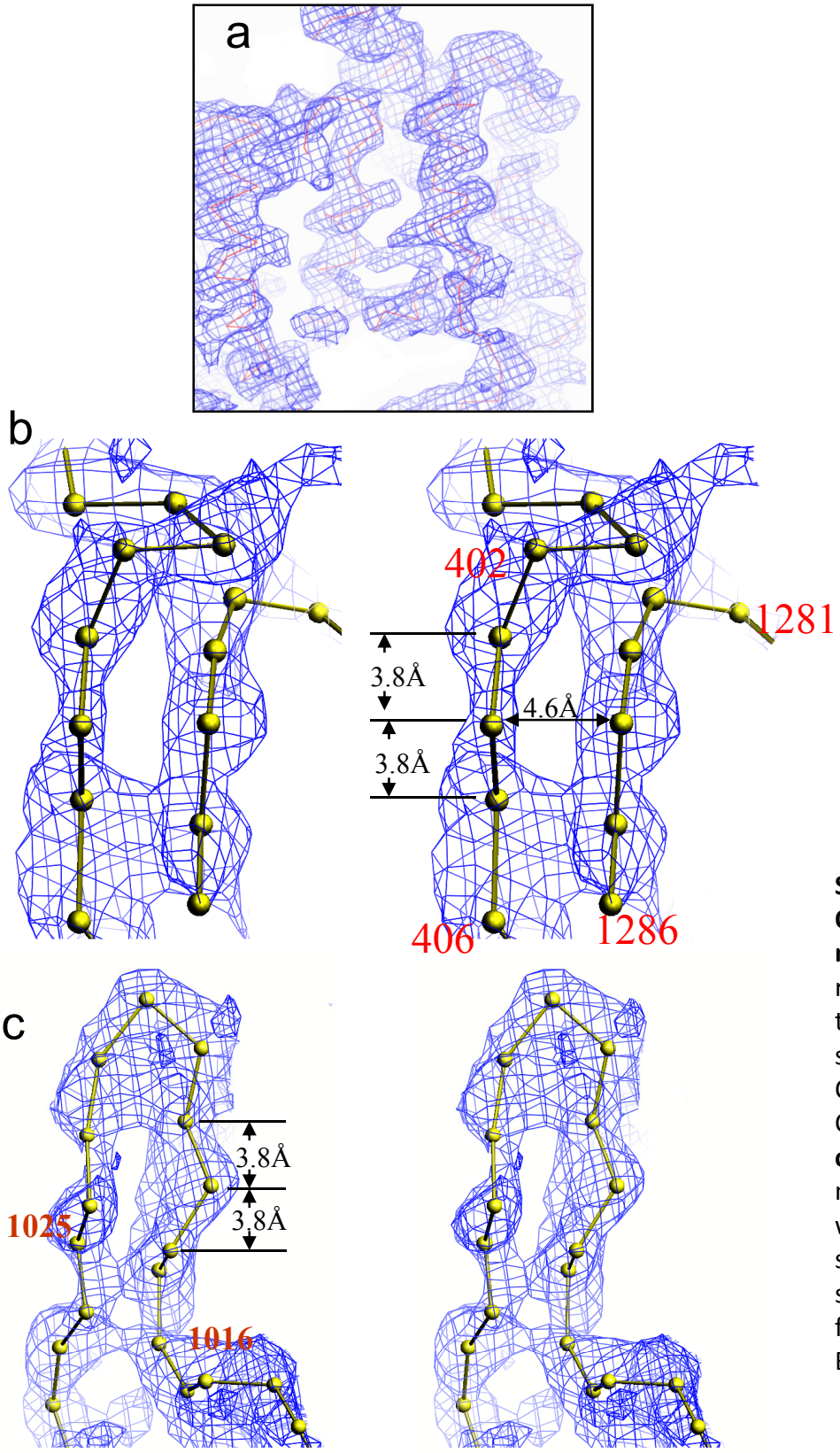

Supplementary Figure 2 Quality of our density maps. a, A representative region of the density map (blue) superimposed with the Cα model (red) of the CSP-B apical domain. **b, c**, Stereo views of Cα models superimposed with density maps, showing the clear separation of β-strands from CSP-A (**b**) and CSP-B (**c**).

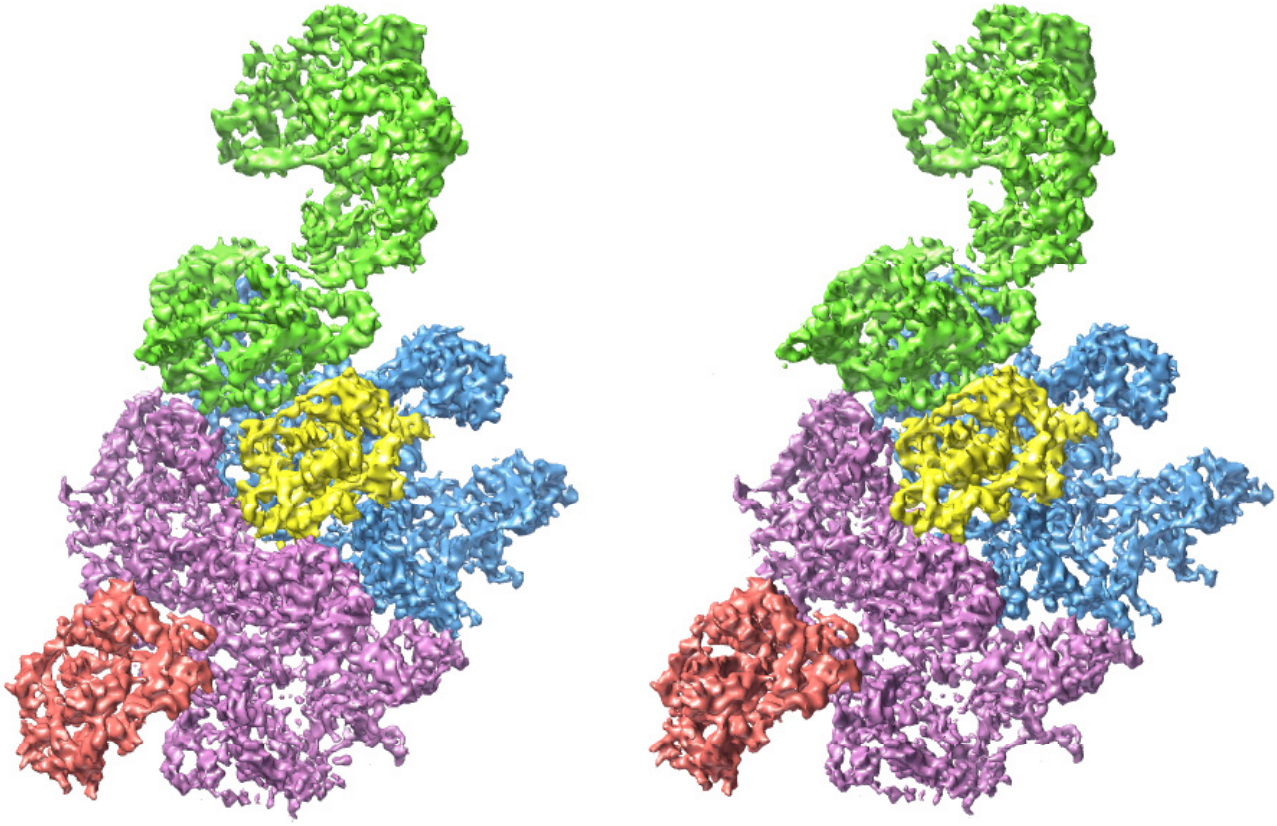

Supplementary Figure 3 Stereo view of an extracted asymmetric unit from the 3.88 Å resolution density map.

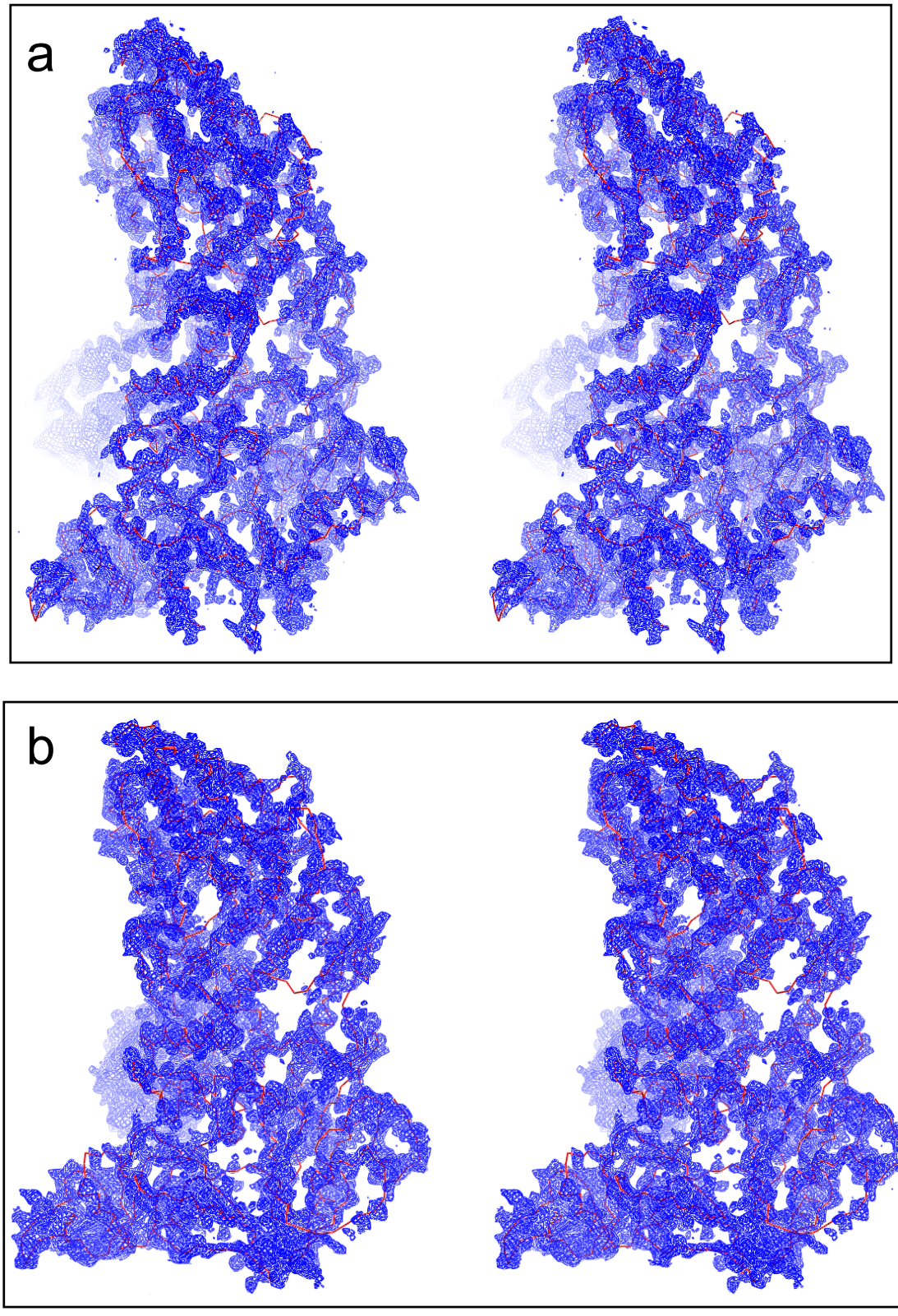

Supplementary Figure 4 Stereo views of Cα models superimposed with the CSP-A (a) and CSP-B (b) density maps.

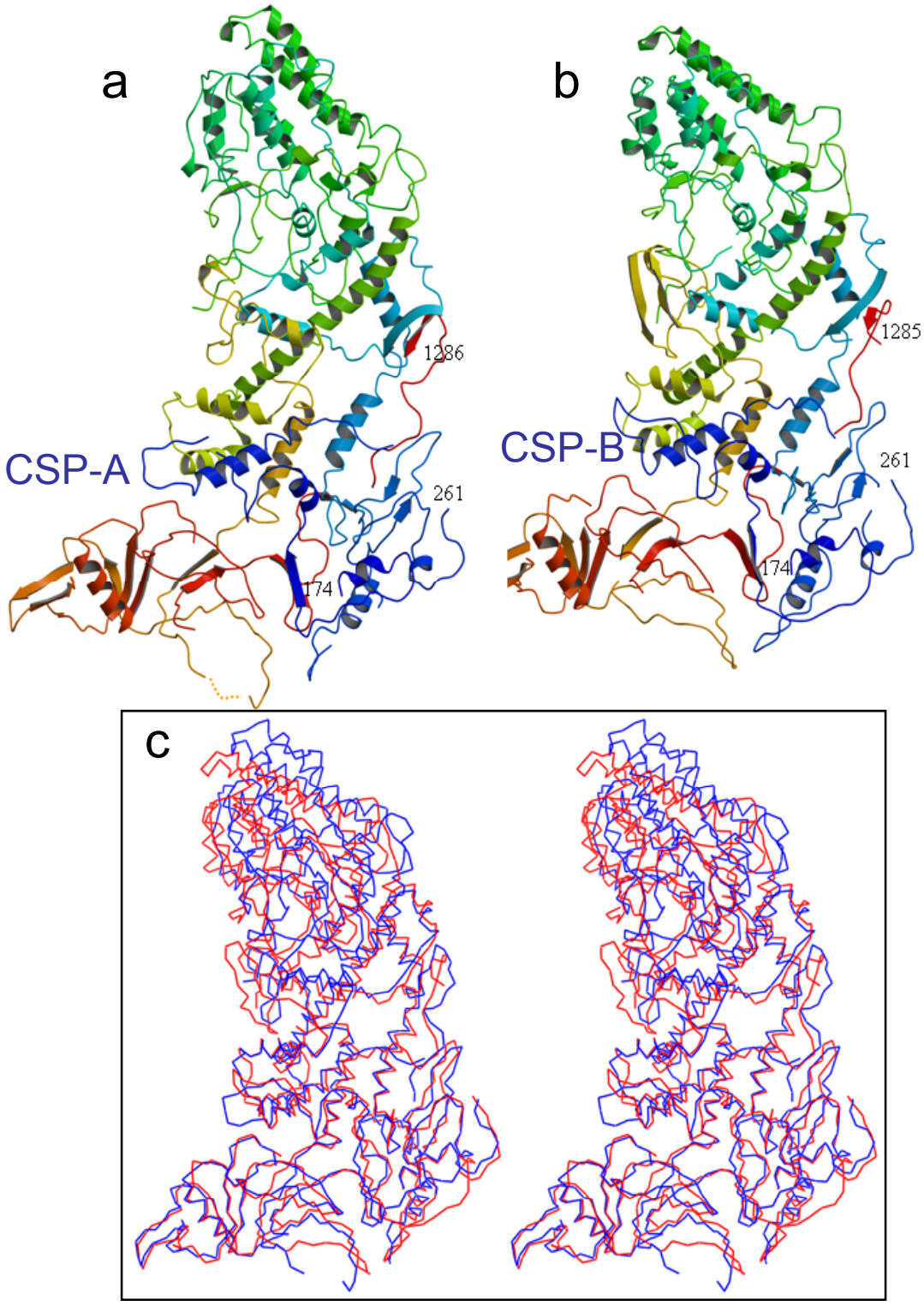

Supplementary Figure 5 Comparison of the Cα models of CSP-A and CSP-B. a, **b**, Atomic models of CSP-A (**a**) and CSP-B (**b**). Figures were made by Molscript[3] and colored from blue at the N terminus to red at the C terminus. **c**, Stereo view of the superposition of CSP-A (blue) and CSP-B (red) Cα traces, showing the overall similarity between CSP-A/CSP-B and the pivot movement between the upper and lower two domains, similar to two λ1 molecules in the orthoreovirus core[4].

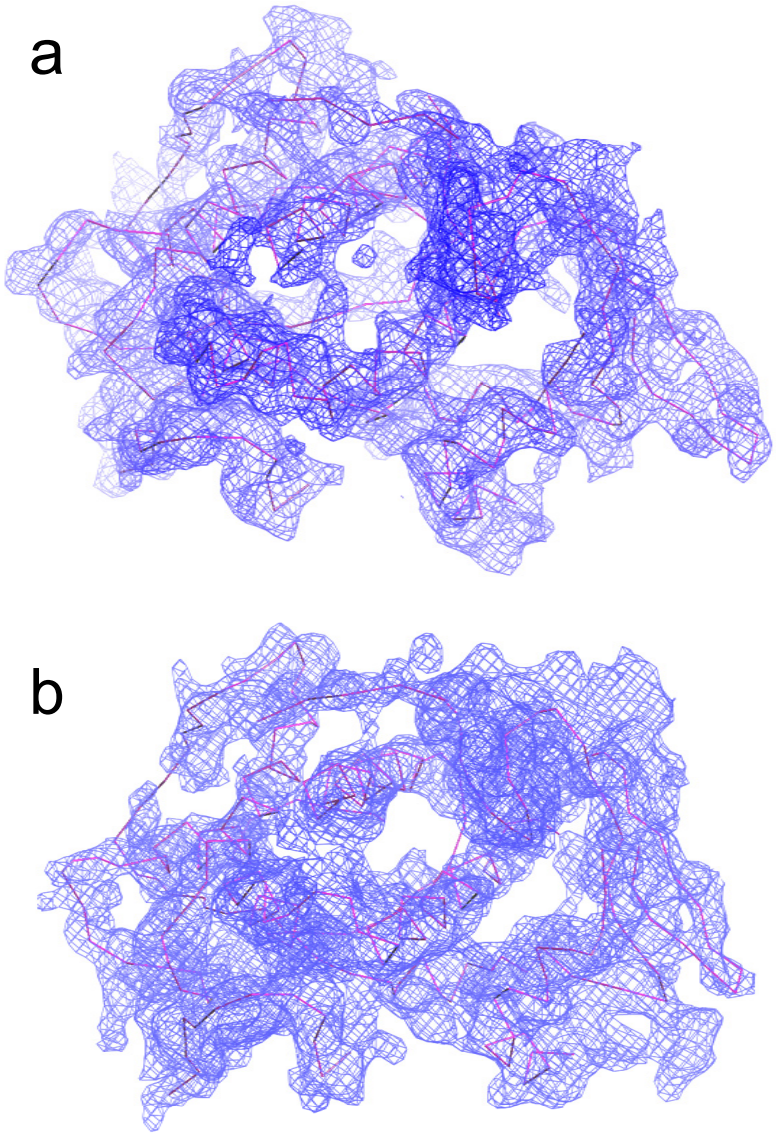

Supplementary Figure 6 **Cα models superimposed with the LPP-5 (a) and LPP-3 (b) density maps.**

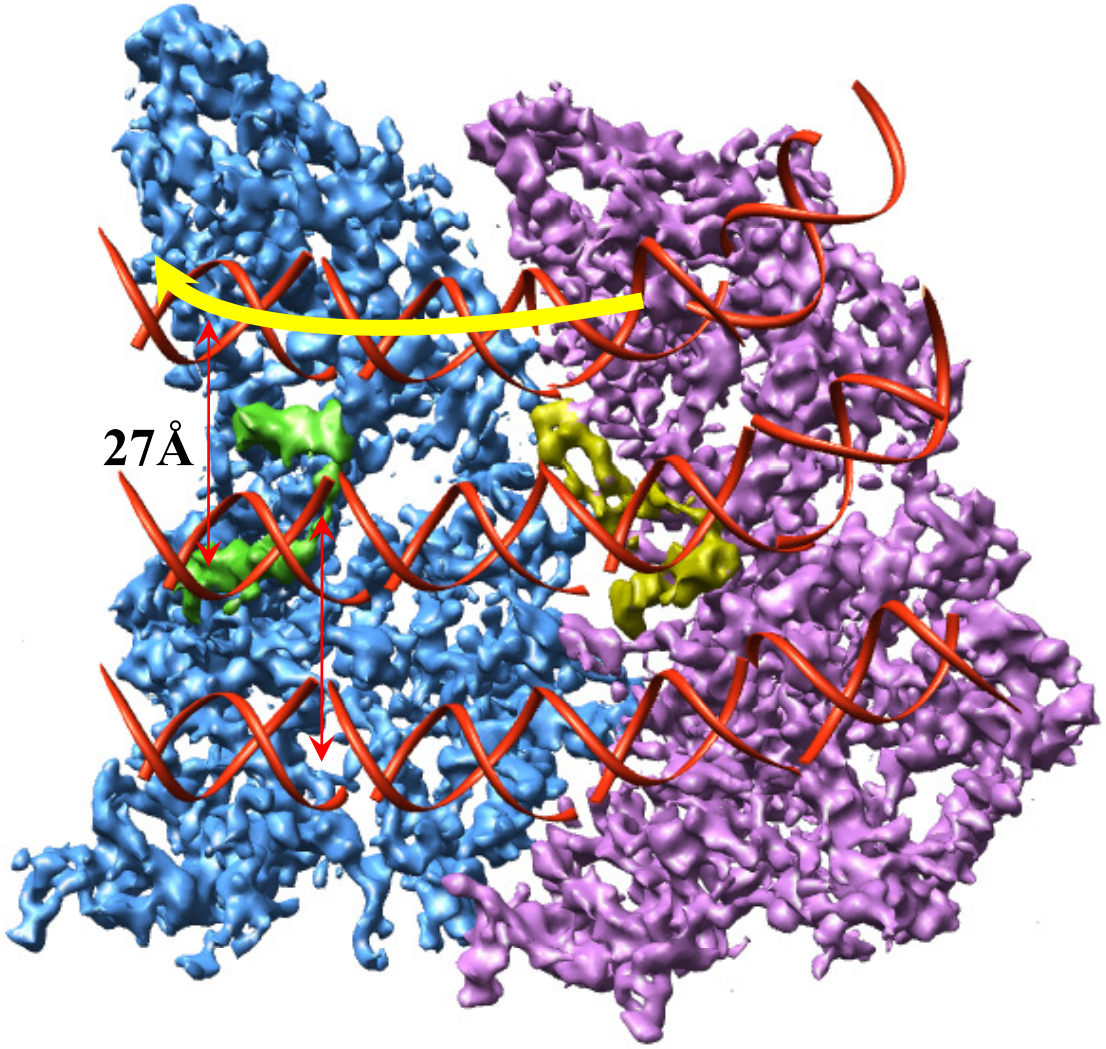

Supplementary Figure 7 Proposed model for dsRNA (red ribbons) packing against CSP-A (blue) and CSP-B (purple), showing three shallow grooves in the inner sides of both CSP-A and CSP-B with a distance of ~27 Å between two adjacent grooves (red arrows). All three grooves are well aligned between CSP-A and CSP-B. We speculate that these grooves may function as tracks for RNA packing and sliding during capsid assembly and mRNA transcription. The changing path indicated in Fig. 4b might correspond to the direction of RNA sliding during replication or transcription (yellow arrow).

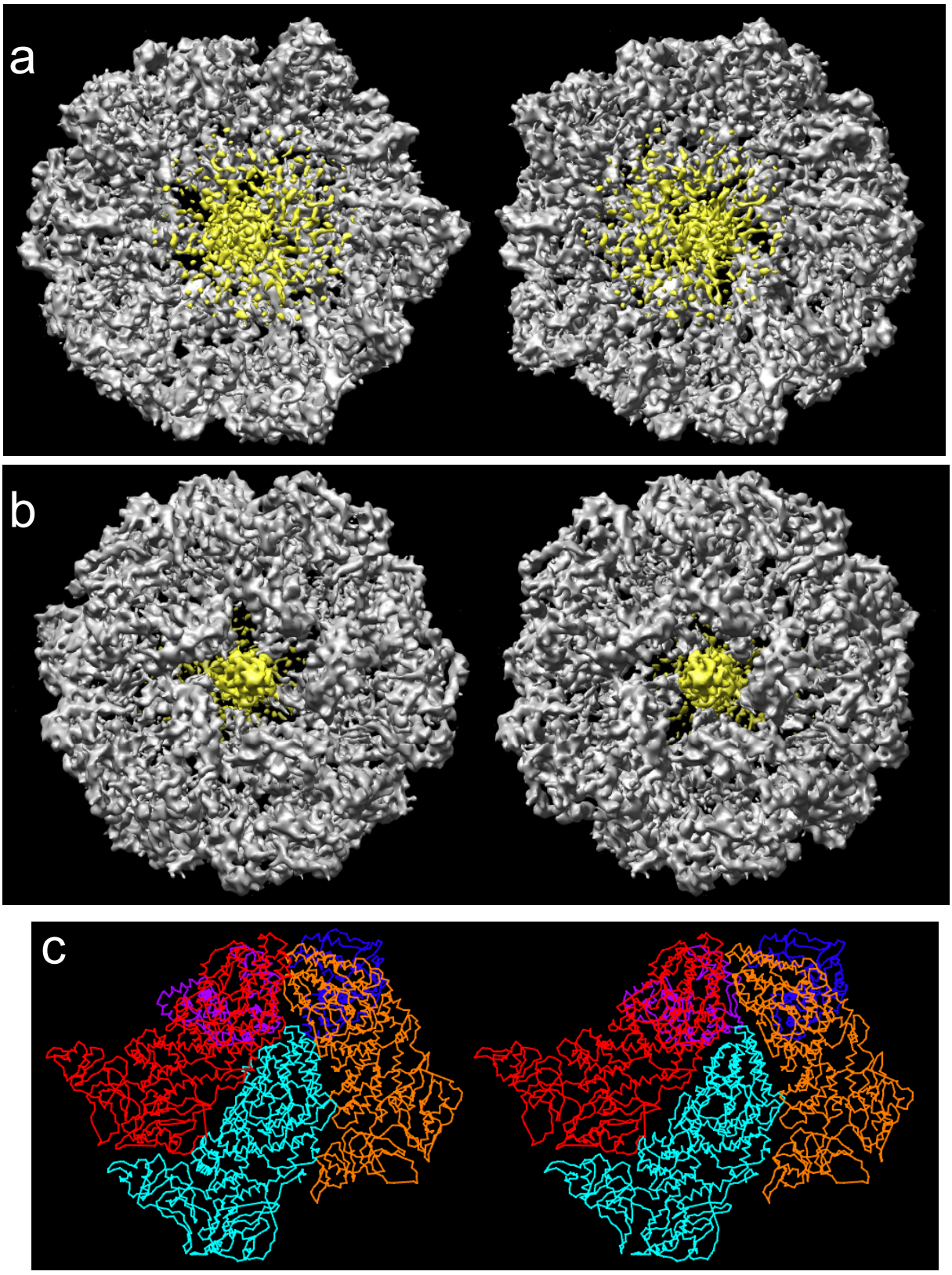

Supplementary Figure 8 Nascent mRNA release hole coupled with the guanylyltransferase (GTase) active site of TP. a, **b**, Stereo views of a TP pentamer viewed from top (**a**) and bottom (**b**) along a 5-fold axis, showing the central chamber of the turret is plugged by the A-spike (yellow density, 1σ). **c**, Stereo view of Cα models of one CSP-B (cyan), two copies of CSP-A (red and orange), and two GTase domains (blue and light blue), showing the mRNA releasing and capping pathway.

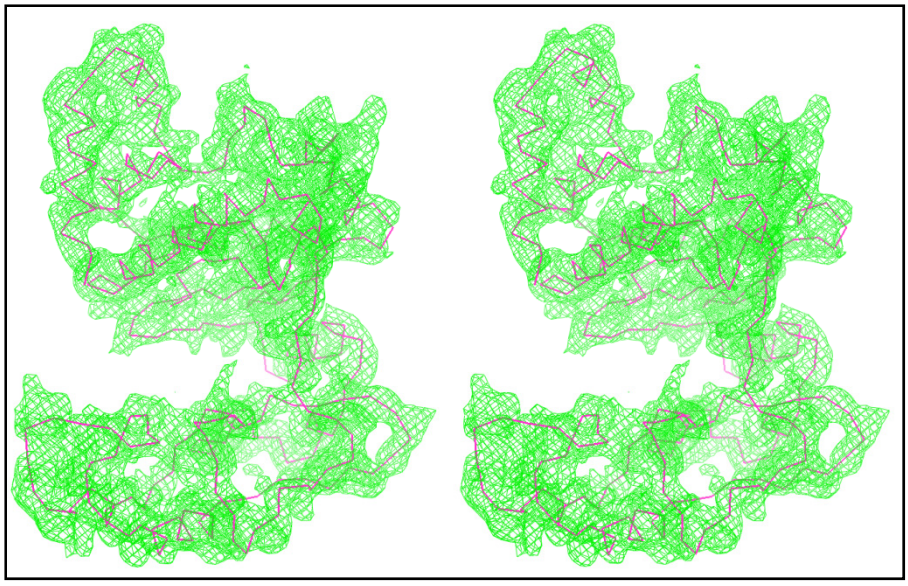

Supplementary Figure 9 **Stereo view of the GTase Cα model superimposed with density map.**

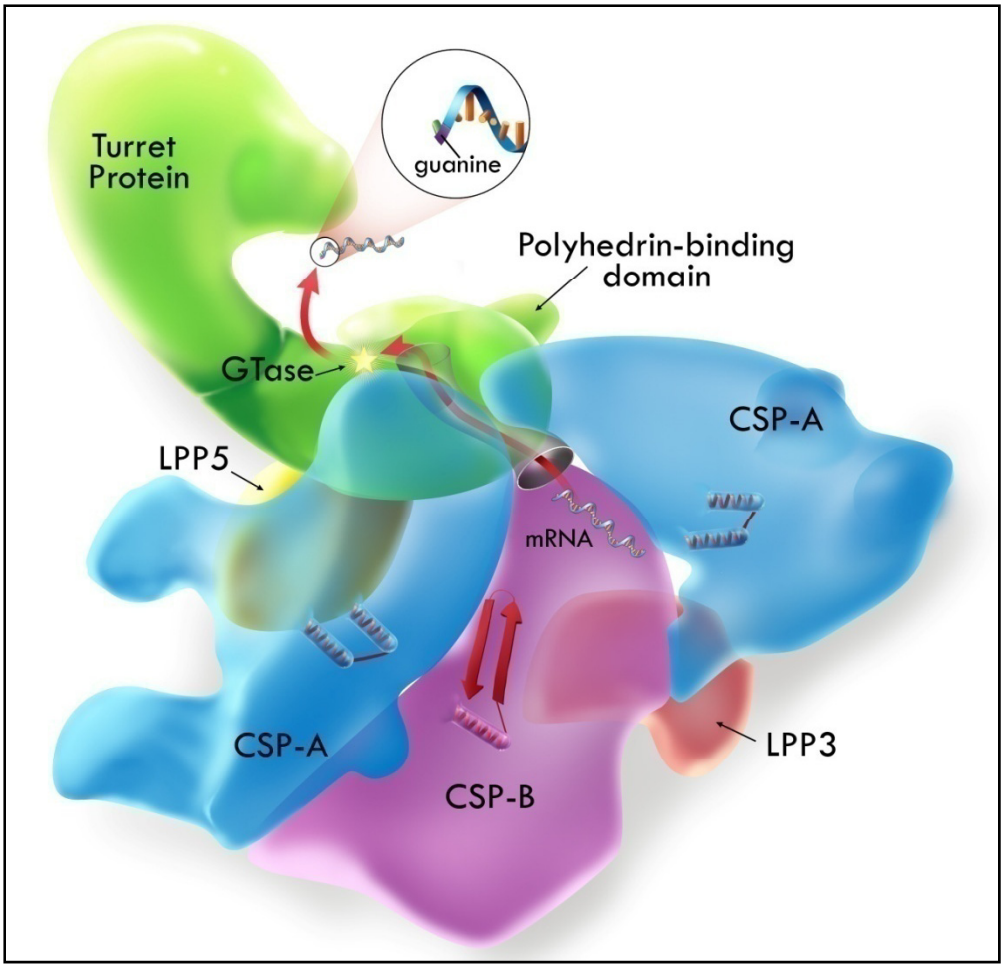

Supplementary Figure 10 Schematic illustration of the functional implications arising from our cryoEM structure. Key findings include a drastic conformational change in the RNA-interacting region between CSP-A and CSP-B, the mRNA releasing and capping pathway, and the unique polyhedrin-binding domain.